Case Studies in Construction Materials 20 (2024) e03207

Contents lists available at ScienceDirect

Case Studies in Construction Materials

journal homepage: www.elsevier.com/locate/cscm

Case study

Anti-cracking and shrinkage performance of sustainable concrete incorporating high-volume natural pozzolans: A case design for high-speed railway concrete slab tracks

Fulin Qu [a,b,*], Yilin Su [a,*], Dong Lu [a], Ning Li [c], Xiaohui Zeng [d], Wengui Li [b]

[a] Department of Civil and Environmental Engineering, The Hong Kong Polytechnic University, Hung Hom, Kowloon, Hong Kong, China
[b] Centre for Infrastructure Engineering and Safety, School of Civil and Environmental Engineering, University of New South Wales, NSW 2052, Australia
[c] Department of Solids and Structures, University of Manchester, Manchester M13 9PL, United Kingdom
[d] School of Civil Engineering, Central South University, Changsha 410075, China

ARTICLE INFO

Keywords:
Nature pozzolans
High-volume substitution
Sustainable
High railway
Shrinkage performance

ABSTRACT

This investigation was conducted to examine the effect of the designed composite agent (DCA) on the shrinkage performance of the concrete high-volume natural pozzolans (PHVNC). Based on an economic-cost analysis, it was determined that natural pozzolans (NP) were a suitable replacement for fly ash (FA) in the production of sustainable concrete for high-speed railway concrete slab track design. The results confirmed that the inclusion of DCA effectively improved the early-age shrinkage performance of PHVNC with 30% or 50% NP content. As a result, the concrete containing high-volume NP and DCA (PHVNDC) exhibited a smaller crack density compared to PHVNC, and even outperformed concrete with a high volume of FA (PHVFC). In terms of the effect of DCA on the drying shrinkage performance of mixes containing NP, a similar trend was observed, where the mixes that included both NP and DCA exhibited lower levels of dry shrinkage and mass loss at 28 days compared to mixes with either NP or FA. The results from phase transformation and microstructure analysis further indicated that adding DCA can enhance the mechanical and shrinkage performance of the mixes containing high-volume NP. This enhancement is attributed to the optimization of the hydration reaction rate, increased production of hydration products, and an overall improvement in the microstructure performance of the mixes with NP. Hence, DCA can serve as a valuable support in preserving the characteristics of NP-based mixtures, making it a valuable discovery for implementing high-volume NP in practical engineering projects with abundant NP resources.

1. Introduction

Currently, Supplementary cementitious materials (SCMs), including fly ash (FA), metakaolin (MK), ground granulated blast-furnace slag (GGBFS), red mud, and others, have emerged as vital substitutes for ordinary Portland cement (OPC) in mortar and concrete production [1–3]. SCMs, rich in amorphous silica, alumina, and calcium oxide (CaO), enhance concrete's mechanical strength and durability through their combined pozzolanic reactivity [4–6]. Furthermore, replacing cement with SCMs significantly reduces

* Correspondence to: The Hong Kong Polytechnic University, Hung Hom, Kowloon, Hong Kong, China.
E-mail addresses: Fulin.qu@polyu.edu.hk (F. Qu), seusy@163.com (Y. Su).

https://doi.org/10.1016/j.cscm.2024.e03207
Received 12 February 2024; Received in revised form 14 April 2024; Accepted 22 April 2024
Available online 23 April 2024

carbon dioxide emissions, directly addressing the environmental issues associated with OPC production, which is notorious for its 1:1 ratio of CO_2 emissions per ton of cement, exacerbating global warming, climate change, and ozone depletion [7,8]. Given its advantages in enhancing overall performance and mitigating global warming potential, the extensive use of high-volume SCMs as a substitute for OPC in concrete production is indispensable for promoting environmentally friendly and sustainable construction practices in infrastructure and high-speed railway engineering projects around the world.

Despite their benefits, the availability of SCMs such as fly ash, a by-product of thermal power plants, is becoming increasingly constrained at some construction sites due to the closure of coal plants as part of green energy transformations, leading to higher costs and environmental impacts from transportation [9–11]. This challenge highlights the importance of identifying alternative, locally accessible materials with pozzolanic reactivity [12–14]. For example, in the Dali-Ruili high-speed railway project in Yunnan Province, the lack of thermal power production limits FA availability. Conversely, the region is rich in natural pozzolans (NP) (in Fig. 1.), offering a more cost-effective and locally sourced alternative at RMB 200 per ton compared to the higher costs associated with transporting FA. However, the activity index of NP is generally lower than that of FA, necessitating further research to optimize the use of NP in concrete production. To ensure the widespread use of NP in practical engineering projects, further research is essential to explore methods for enhancing the performance of concrete with high NP content [14–16].

Recent decades have seen efforts to enhance the performance of concrete using high-volume natural pozzolans (PHVNC) [17–20]. Celik et al. [21,22] incorporated 15 wt% limestone powder to enhance the performance of concrete with 35 wt% NP, resulting in excellent one-year strength and high chloride penetration resistance in the designed concrete. Sharbaf et al. [23] utilized various dosages of FA to improve the abrasion resistance of PHVNC. Their research revealed that the concrete with the addition of 22.5 wt% FA and 15 wt% NP displayed the best abrasion resistance performance. Ahmad et al. [24] employed microsilica to optimize the performance of ultra-high-performance concrete (UHPC) with high-volume NP content. They reported that all designed mixtures containing natural pozzolan met the requirements for UHPC in terms of modulus of elasticity, splitting tensile strength, and fracture toughness. However, it is important to highlight that the research mentioned above [17–24] primarily focused on the mechanical and durability aspects of PHVNC. There has been limited exploration of the shrinkage performance of PHVNC in the existing literature. The shrinkage behavior is an inherent characteristic of cement-based materials, occurring in both the plastic and hardened stages [25–28]. As a result of shrinkage, tensile stresses caused by non-uniform deformation within the material can easily lead to detrimental cracking. These cracks, in turn, provide pathways for aggressive agents like chlorides and sulphates to penetrate the material, ultimately compromising the long-term durability and serviceability of the structure [29,30]. Therefore, addressing shrinkage behavior is crucial for ensuring the longevity and safety of concrete structures.

In this context, with the focus on the application of PHVNC designed for the high-speed railway concrete slab track (as illustrated in Fig. 2), two distinct concrete classes, namely C20 and C40, were developed for this study. The C20 class concrete was tailored for use in the hydraulically stabilized base (HSB), while the C40 class concrete was formulated for manufacturing the track concrete layer (TCL). Moreover, in light of the consideration of implementing NP as a replacement for FA in practical projects and assessing its feasibility, a specially designed composite agent (DCA) was also employed to enhance the shrinkage performance of PHVNC. Herein, considering the application of PHVNC designed for the high-speed railway concrete slab track (as shown in Fig. 2), two different concrete classs (C20 and C40) were also designed in this study. Employing NP as a substitute for FA and using a designed composite agent (DCA) aims to enhance the shrinkage performance of PHVNC. Primary research methods include the Kraai modified test for early-age shrinkage performance, along with evaluations of mechanical and drying shrinkage properties of mortar mixes with high-volume SCMs [31,32].

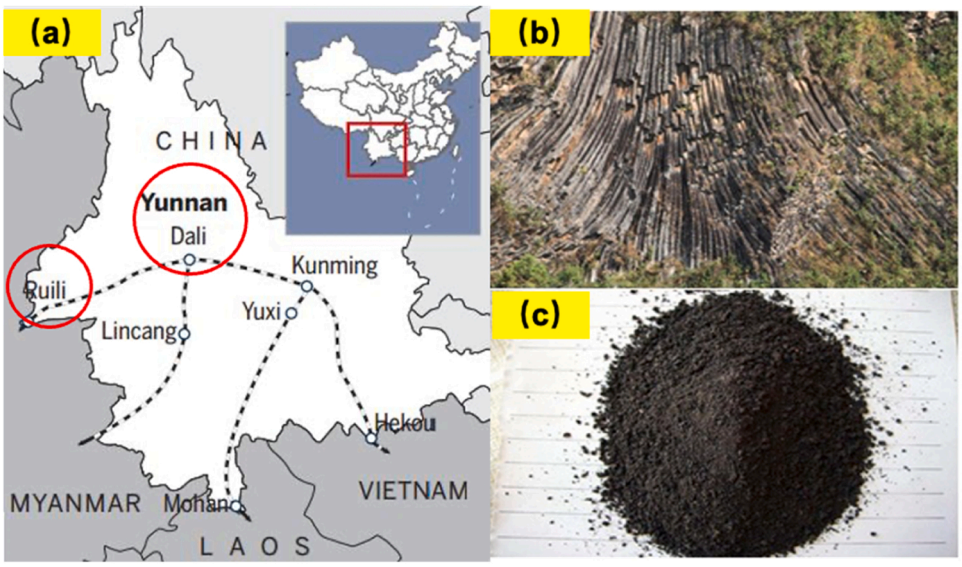

Fig. 1. The distribution of NP resources along the Dali-Ruili railway in Yunnan Province, China: (a) The railway line distribution in Yunnan Province, (b) Resources of NP, and (c) NP used in this study.

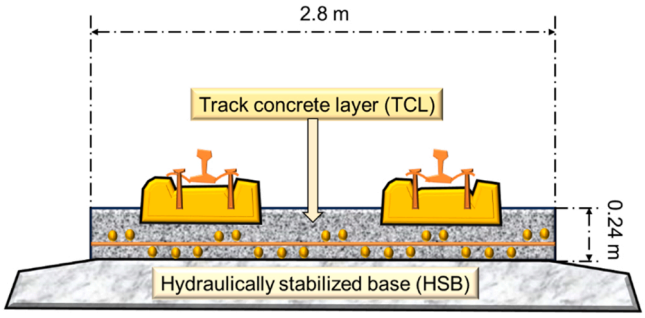

Fig. 2. Slab track systems for high-speed railways.

Additionally, the study examines the phase transformations and microstructure of mixes with high NP content through resistivity, differential thermal analysis (DTA), and scanning electron microscopy (SEM). The findings are expected to provide comprehensive support for using high-volume NP in high-speed railway design, contributing to sustainable construction practices.

2. Experimental program

2.1. Raw materials

In this study, the following materials were employed: 42.5 R Ordinary Portland cement (OPC), provided by Yunnan Conch Cement Co., Ltd, China; Class F fly ash (FA) sourced from Sichuan Suining Materials Co., Ltd, China; and natural pozzolan (NP) supplied by Yunnan Jiangteng Co., Ltd, China. The FA had a fineness of 45 μm, a square sieve residue of 18.4%, a water demand ratio of 104%, a burn loss of 6.73%, and an activity index of 70.2%. Additionally, the NP had a fineness of 45 μm, a square sieve residue of 20%, a loss on ignition of 1.18%, an activity index of 75.3%, and a mobility of 1.04. The particle size distribution of OPC, FA, and NP is presented in Fig. 3, with FA and NP being finer than OPC.

The chemical composition of OPC, FA, and NP, as determined by XRF, is also detailed in Table 1. Furthermore, river sand with a fineness modulus of 3.36 was used as fine aggregate, and continuously graded crushed stone ranging from 5 to 31.5 mm served as coarse aggregate in this study. A solid DCA, comprising silica fume, polyvinyl alcohol, polycarboxylic acid powder, rubber powder, and other components, was employed to enhance the shrinkage performance of PHVNC. The specific details of the DCA can be found in Table 2. It should be noted that the DCA discussed in this article utilizes exclusively solid powder materials and is formulated from all solids to facilitate construction convenience, drawing on the extensive construction experience of our research team. In addition, both tap water and deionized water (utilized for the resistivity test) were employed as part of the experimental setup.

2.2. Mix proportion

For the assessment of cracking performance, two distinct classes of concrete mixes with varying water-to-binder (W/B) ratios were prepared in this study. Each concrete mix comprised four different types, as detailed below: concrete with OPC (PC group), concrete

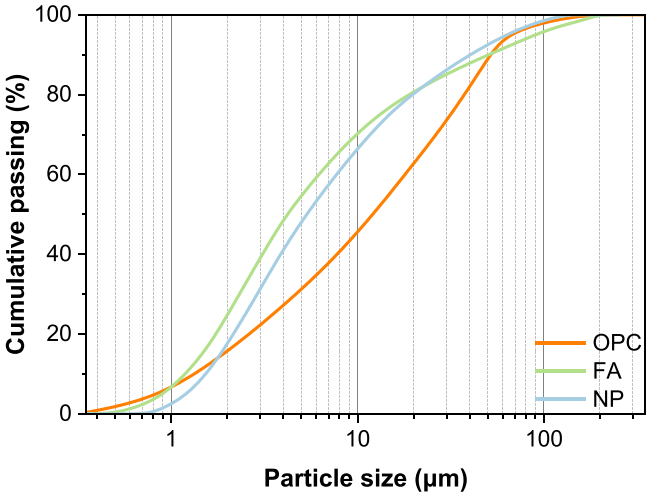

Fig. 3. Particle size distribution of OPC, FA and NP.

Table 1
Chemical compositions of raw materials (wt%).

Types	SiO_2	Al_2O_3	Fe_2O_3	CaO	MgO	Na_2O	K_2O	SO_3	LOI
OPC	21.45	5.75	2.89	61.123	1.54	0.77	0.81	2.66	3.08
FA	55.65	32.92	5.18	2.48	0.43	0.28	0.05	0.04	3.51
NP	59.51	17.27	5.34	7.25	3.49	3.98	2.18	0.05	3.37

Table 2
The details of composite agent (%).

Silica fume	Water retaining agent	Polyvinyl alcohol	Polycarboxylic acid powder	Rubber powder
90.5 %	1.0 %	3.5 %	1.5 %	3.5 %

with high-volume FA (PHVFC group), concrete with high-volume NP (PHVNC group), and concrete with NP and DCA (PHVNDC group). Within each type of concrete mix with a W/B ratio of 0.49, four variations were manufactured, as follows: Ordinary Portland Cement concrete with a W/B ratio of 0.49 (PC1), concrete with 50.0 wt% of FA (PHVFC1), concrete with 50.0 wt% NP (PHVNC1), and concrete with 50.0 wt% NA and 3.0 wt% DCA (PHVNAC1). In addition, another type of concrete with a W/B ratio of 0.38 included four variations: Ordinary Portland Cement concrete (PC2), concrete with 30.0 wt% of FA (PHVFC2), concrete with 30.0 wt% NA (PHVNC2), and concrete with 30.0 wt% NA and 3.0 wt% DCA (PHVNAC2). It is worth noting that FA and NA were utilized as binder materials to replace OPC. In contrast, an additional 3% by mass of binder materials in the form of DCA was incorporated into the PHVNAC group, such as PHVNAC1 and PHVNC2. The mix proportions for 1 m^3 of concrete were calculated based on the Chinese standard GB/T50476–2008 (Specification for durability design of concrete structures) and are presented in Table 3. Furthermore, mortar and paste specimens were also prepared by adjusting the mix proportions outlined in Table 3.

2.3. Test procedures

Fig. 4 illustrates the comprehensive range of test procedures. As depicted in Fig. 4, concrete specimens were utilized for conducting the crack test to evaluate the early-age shrinkage performance of concrete with NP. Mortar specimens were employed to assess drying shrinkage, mass loss, and mechanical performance, providing further insights into the shrinkage performance of mortar with NP. Paste

Table 3
Mixing proportions of concrete, mortar, and paste (Kg/m^3).

Concrete mix proportion							
Mix ID	**OPC**	**FA**	**NP**	**Water**	**Sand**	**Gravel**	**DCA**
PC1	333	—	—	163	829	1055	—
PHVFC1	166.5	166.5	—	163	829	1055	—
PHVNC1	166.5	—	166.5	163	829	1055	—
PHVNAC1	166.5	—	166.5	163	829	1055	9.99
PC2	429	—	—	163	809	1029	—
PHVFC2	300	129	—	163	809	1029	—
PHVNC2	300	—	129	163	809	1029	—
PHVNAC2	300	—	129	163	809	1029	12.87
Mortar mix proportion							
Mix ID	**OPC**	**FA**	**NP**	**Water**	**Sand**	**DCA**	
PM1	333	—	—	163	829	—	
PHVFM1	166.5	166.5	—	163	829	—	
PHVNM1	166.5	—	166.5	163	829	—	
PHVNAM1	166.5	—	166.5	163	829	9.99	
PM2	429	—	—	163	809	—	
PHVFM2	300	129	—	163	809	—	
PHVNM2	300	—	129	163	809	—	
PHVNAM2	300	—	129	163	809	12.87	
Paste mix proportion							
Mix ID	**OPC**	**FA**	**NP**	**Water**	**DCA**		
PP1	333	—	—	163	—		
PHVFP1	166.5	166.5	—	163	—		
PHVNP1	166.5	—	166.5	163	—		
PHVNAP1	166.5	—	166.5	163	9.99		
PP2	429	—	—	163	—		
PHVFP2	300	129	—	163	—		
PHVNP2	300	—	129	163	—		
PHVNAP2	300	—	129	163	12.87		

Note: ‘C’ in PC1 stands for concrete; ‘M’ in PM1 stands for mortar; The second ‘P’ in PP1 stands for paste; PM stands for the Portland cement mortar; PP stands for the Portland cement paste; Other mortars or pastes are named in the same way as concrete.

mixes were utilized to conduct microstructural performance evaluations, including non-contact resistibility tests, DTA, and SEM analysis, to provide additional explanations regarding the influence of NP on the shrinkage performance of concrete with NP.

2.3.1. Crack observation

The testing for early shrinkage cracking in concrete was conducted using a double-restrained steel slab mould, known as the Kraai modified test. The mould had dimensions of 800 mm × 600 mm × 100 mm, as depicted in Fig. 5. Further details regarding the steel mould are provided below [31,32]: The mould consists of four sides, including the long side plate and the short side plate, which were welded with angle steel having a thickness of 5 mm; Bolts were used to securely fasten the four sides of the mould to the bottom plate; The mould was equipped with seven crack inducers, each made of 50 × 50 mm and 40 × 40 mm angles welded together with 5 × 5 mm steel plates, where these inducers were oriented parallel to the short side of the mould; The base plate of the mould was constructed using a 5 mm thick steel plate, and a polyethylene film sheet was placed on the surface of the base plate to serve as an isolation layer; To increase the risk of cracking, a 5 m/s air flow supplied by a calibrated fan was directed onto the slab, as illustrated in Fig. 5(b).

Where preparing the concrete specimens, the steel moulds were first moved to a constant temperature and humidity room with a temperature of 20 ± 2 ℃ and a relative humidity of 60 ± 5%; And then, the concrete mixtures were prepared based on the Chinese standard GB/T 50082–2009 (Standard for test methods for long-term performance and durability of ordinary concrete); Following that, the mixed concrete was poured into the mould, vibrated for 3 times with about 30 s for each time, and its surface was smoothed with a trowel; After the specimen is formed for 30 min, two calibrated fans with a 5 m/s air flow were vertically placed at 100 mm above the center of the specimen surface to ensuring the wind direction being parallel to the surface, as shown in Fig. 5(b); Finally, after the 24 h (calculated from adding the water), the length of the crack was measured with a steel straightedge and the maximum width of each crack was measured using a reading microscope with a magnification of 40 times, as shown in Fig. 5(c) and (d). Based on the record of crack data (e.g., number of cracks, length of crack and maximum width of crack), the average cracking area, the number of cracks per unit area, and crack density (the total cracking area per total cross-section area) were calculated according to the Equations 1, 2 and 3, as shown in the following:

$$a = \frac{1}{2N}\sum_{i=l}^{N}(W_i \times L_i) \tag{1}$$

$$b = \frac{N}{A} \tag{2}$$

$$c = a \times b \tag{3}$$

Where W_i stands for the maximum width of the crack of number i (mm); L_i stands for the length of the crack of number i; N stands for

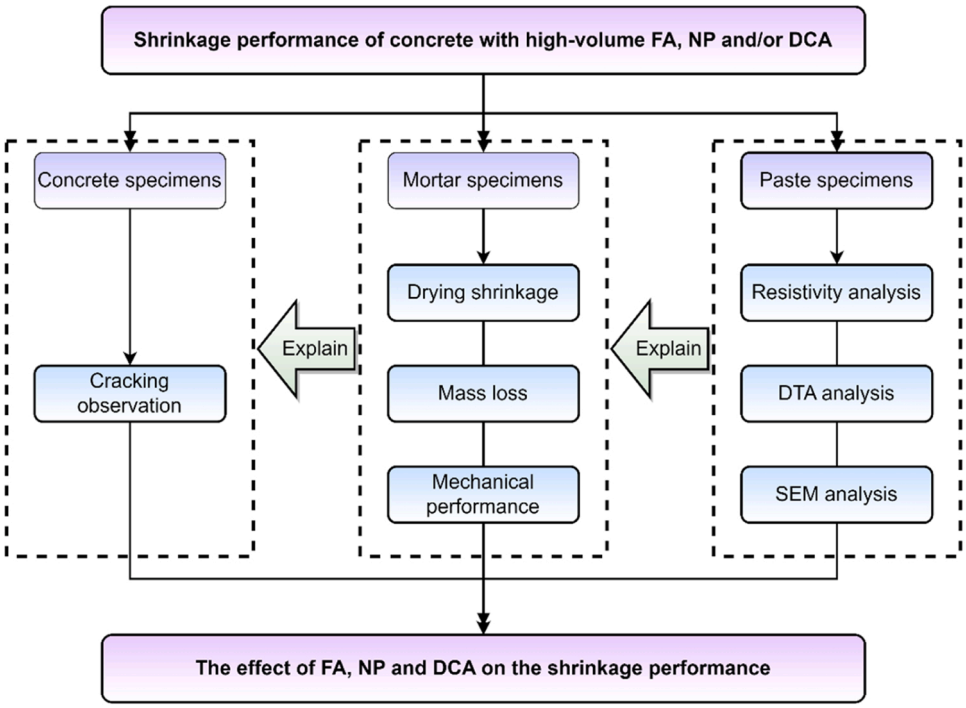

Fig. 4. Full scope of the test procedures.

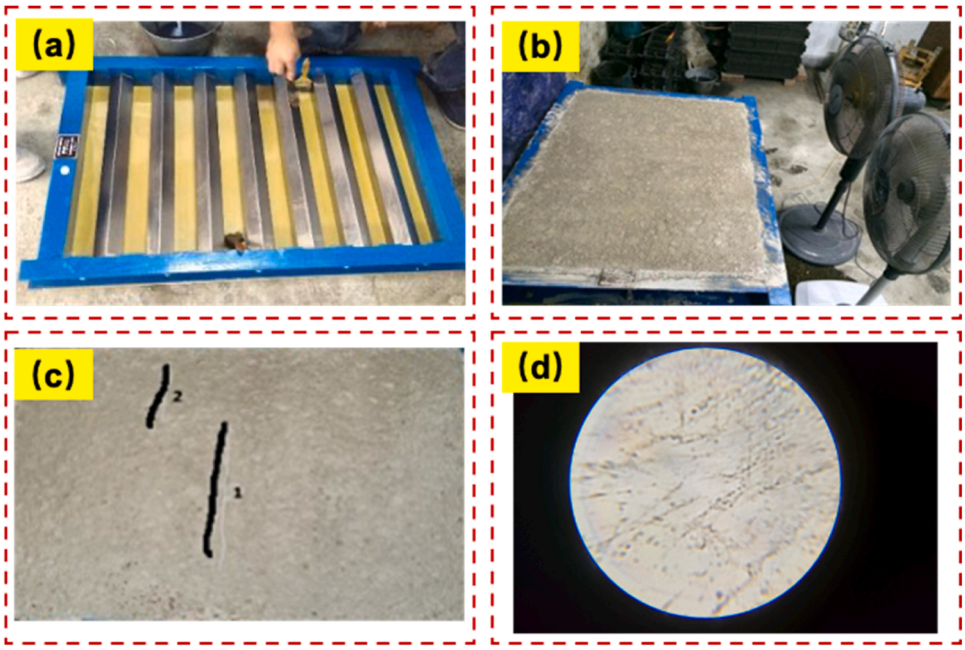

Fig. 5. Set-up for early-age shrinkage cracking test (a) test mould, (b) test with calibrated fans, (c) image acquisition, (d) microscope with a magnification of 40 times.

the number of cracks; *A* stands for the area of the slab (m^2); *a* stands for the average cracking area of each crack; b stands for the number of cracks per unit area; and c stands for the crack density (the total cracking area per total cross-section area) (mm^2/m^2). In this section, the total cracking area per unit area was the average result of three concrete specimens.

2.3.2. Drying shrinkage and mass loss measurement

According to the Chinese standard JC/T 603–2004 (standard test method for drying shrinkage of mortar), the mortar for drying shrinkage and mass loss test were manufactured using a mould with a dimension of 25×25×280 mm. After being cured at the standard conditions at a temperature of 20 ± 1°C and relative humidity of 95% for 24 h, the original length (L_o) and weight (W_o) of the mortar specimens were measured by a micrometre with an accuracy of 0.001 mm and a scale with an accuracy of 0.001 g, respectively. After that, the specimens were kept in a drying curing condition at a temperature of and % relative humidity of 50% until the different test ages, including 3, 5, 7, 14, 21 and 28 days. The length and weight of each mortar specimen under different test ages were also measured. The drying shrinkage (S_i) and mass loss (W_i) were calculated based on the following Equations 4 and 5. In this section, the values of drying shrinkage and weight recorded were the average results of three specimens.

$$S_i = \frac{L_o - L_i}{L_o} \tag{4}$$

$$W_i = \frac{W_o - W_i}{W_o} \tag{5}$$

where L_o was the original length of the different mortar specimens (mm); L_i was the length of the corresponding mortar specimens recorded at different test ages (mm); W_o was the original weight of the different mortar specimens (g), and W_i was the weight of the corresponding mortar specimens recorded at the test days (g).

2.3.3. Mechanical performance measurement

Based on the Chinese standard JGJ/T 70–2009 (Standard for test methods for mechanical properties of cement mortars), the mortar specimens for strength measurement, including compressive and flexural strength tests, were cast using a mould with a dimension of 40×40×160 mm. After being demoulded, the mortar specimens were cured at the standard conditions with a temperature of 20 ± 1°C and relative humidity of 95% until the test ages (3 or 28 days).

2.3.4. Resistivity measurements using the electrodeless instrument

The electrical resistivity of the studied paste specimens was measured by an electrodeless resistivity apparatus (CCR-III, Hong Kong Brilliant Concept Technologies, China), as shown in Fig. 6. Each paste for resistivity test was mixed via the means in a Chinese Standard GB/T 17671–1999 (Method of testing cements-Determination of strength) and was immediately cast in a ring-shaped plastic mould in

2 min from being mixed with water. Then, the electricity of all paste samples was tested at a testing temperature of 22 ± 2 °C and the resulting data was recorded in a computer for up to 24 h, and the sampling period was two minutes. The principle of the electrical resistivity measurement in question was given in the references [33–35].

2.3.5. DTA measurement

After the electricity test, the paste specimens were kept at the standard condition with a temperature of 20 ± 1°C and relative humidity of 95% for another 27 d. The paste specimen was grounded into powder with a particle size lower than 45 μm. After that, the powder sample was immersed in the anhydrous ethanol and dried in a vacuumed oven for 48 h. Around 30 mg of the powder sample was weighed in an alumina crucible and heated using ZCA-A supplied by Beijing Jingyi Hi-Tech Instrument Co., Ltd. The heating temperature was elevated from 40 °C to 1000 °C at a rate of 10 °C/min in a nitrogen environment [36,37].

2.3.6. SEM analysis

SEM was employed for microstructural analysis using an SEM testing system with a working distance ranging from 5 to 10 mm and a voltage of 30 kV [38,39]. The samples utilized for the SEM test were blocks measuring approximately 2–5 mm in diameter and were taken from the paste samples (aged for 1 day and 28 days). These samples were initially soaked in anhydrous ethanol and then dried in a vacuum oven for 48 h. Prior to the SEM analysis, the samples were coated with a layer of Au/Pd.

3. Results and discussions

3.1. Cracking observation

Fig. 7 presents a typical cracking pattern observed in the concrete specimens. As depicted in Fig. 7, a noticeable difference is evident among the various concrete specimens, attributable to the incorporation of FA, NP, and DCA. Based on the number of cracks, length of crack and maximum width of crack recorded from the concrete surface, crack density calculated based on the above equations was regarded as an essential parameter describing cracking behaviour, as presented in Table 4. Table 4 shows that for concrete mixes with the same W/B ratio, the concrete mixes with NP (e.g., PHVNC1 or PHVNC2) has the highest cracking density, followed by the concrete mix with FA, the concrete mix with NP and DCA, and finally, the reference concrete mix. This suggests that the addition of both FA and NP has a detrimental impact on the early-stage cracking performance of concrete, leading to concrete with FA or NP exhibiting a higher cracking density compared to the reference concrete. Furthermore, the adverse impact of NP is more significant when compared to that of FA, resulting in PHVNC1/PHVNC2 having a higher crack density than PHVFC1/PHVFC2. It is important to note that the incorporation of DCA effectively optimizes the early-age cracking performance of PHVNC. For instance, the PHVNAC1 mix exhibits a crack density of 193 mm^2/m^2, lower than PHVNC1 at 628 mm^2/m^2 and even lower than PHVFC1 at 197 mm^2/m^2.

These phenomena may be attributed to the following reasons: The replacement of OPC by FA or NP reduces the relative content of OPC available for participating in the hydration reaction and optimizing the microstructural performance at an early age; The high-volume inclusion of FA and NP can negatively affect the microstructural properties, resulting in increased moisture evaporation and, consequently, an increase in shrinkage for PHVFC and PHVNC groups; In comparison to spherical FA particles, NP particles have a flat or honeycomb-shaped morphology with numerous edges and corners, which could increase water surface adsorption and reduce the likelihood of hydration reactions, further intensifying the adverse effects on microstructural properties; The addition of DCA serves to optimize the surface of NP and enhances the hydration reaction of OPC, owing to the various components within the DCA, in turn, further optimizes the shrinkage of concrete with high-volume NP.

Moreover, it is evident from Table 4 that within the same concrete group, a higher W/B ratio (or lower concrete class) results in a greater cracking density. This observation can be attributed to the C20 class concrete having a higher content of FA or NP compared to

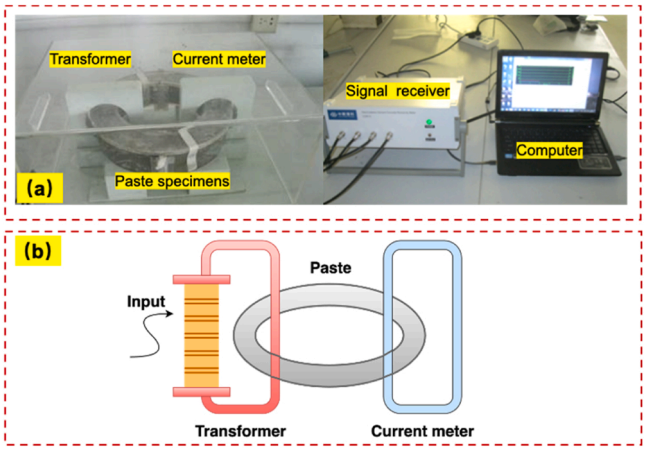

Fig. 6. Electrodeless resistivity instrument: (a) Actual non-contact resistivity instrument and (b) Measurement model.

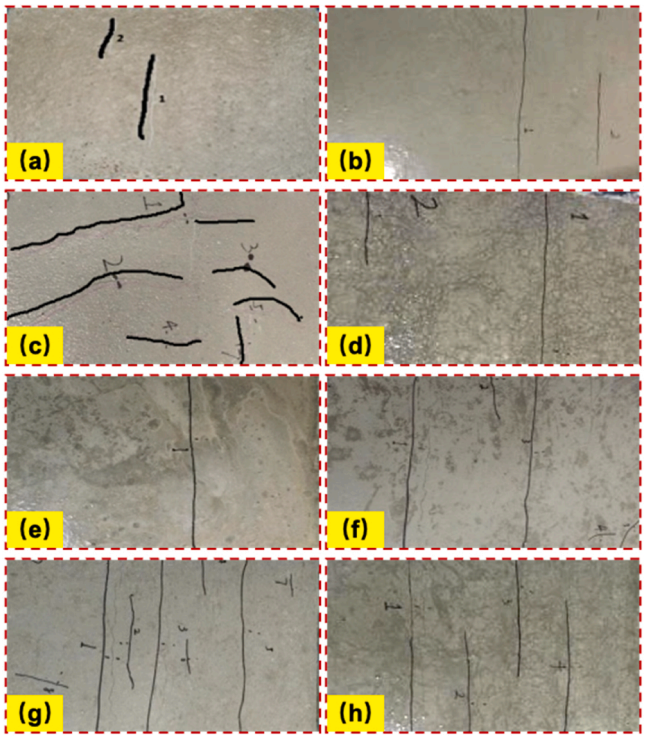

Fig. 7. Cracking pattern of the concrete specimens: (a) PC1, (b) PHVFC1, (c) PHVNC1, (d) PHVNAC1, (e) PC2, (f) PHVFC2, (g) PHVNC2, and (h) PHVNAC2.

Table 4
The crack density of each concrete mix (mm^2/m^2) .

Mix ID	C20 (W/B=0.49)				C40 (W/B=0.38)			
	PC1	PHVFC1	PHVNC1	PHVNAC1	PC2	PHVFC2	PHVNC2	PHVNAC2
Cracking	88	538	735	423	80	197	628	193

the C40 class concrete. This decrease in the relative content of OPC available to participate in the hydration reaction leads to the C20 concrete having a less dense microstructural property in comparison to the C40 concrete. Furthermore, the higher W/B ratio in C20 concrete could also have a more pronounced adverse effect on the microstructural properties. Consequently, the early-age shrinkage performance of C20 concrete is inferior to that of C40 concrete. In summary, while the PHVNAC group still exhibits a higher cracking density than the PC group, the inclusion of DCA allows for the replacement of NP for FA in concrete with relatively higher resistance to early-age cracking. The incorporation of DCA facilitates the promotion and utilization of substantial quantities of NP in sustainable concrete.

3.2. Mass loss and drying shrinkage

Fig. 8 illustrates the mass loss and drying shrinkage of various mortar mixes with different W/B ratios. It is evident from Fig. 8 that, within each group with the same W/B ratio, the inclusion of high-volume FA and NP results in higher mass loss and drying shrinkage in the mortar specimens compared to the reference mortar specimens. This observation could be attributed to changes in the relative cement content. In comparison to the mortar mix with FA, the addition of NP appears to have a more adverse impact on the shrinkage performance, resulting in the mortar mix with NP having the highest mass loss and drying shrinkage.

Additionally, the inclusion of DCA serves to optimize the drying shrinkage in the mortar mix with NP, leading to the mortar mix with NP and DCA (PHVNAM1 or PHVNAM2) exhibiting lower mass loss and drying shrinkage than the mortar mix with NP, and even lower than the mortar mix with FA. Additionally, Fig. 8 also reveals that the mortar with a lower W/B ratio exhibits less mass loss and drying shrinkage than the mortar mix with a higher W/B ratio. This observation may be attributed to the denser microstructure found in the mortar mix with the lower W/B ratio.

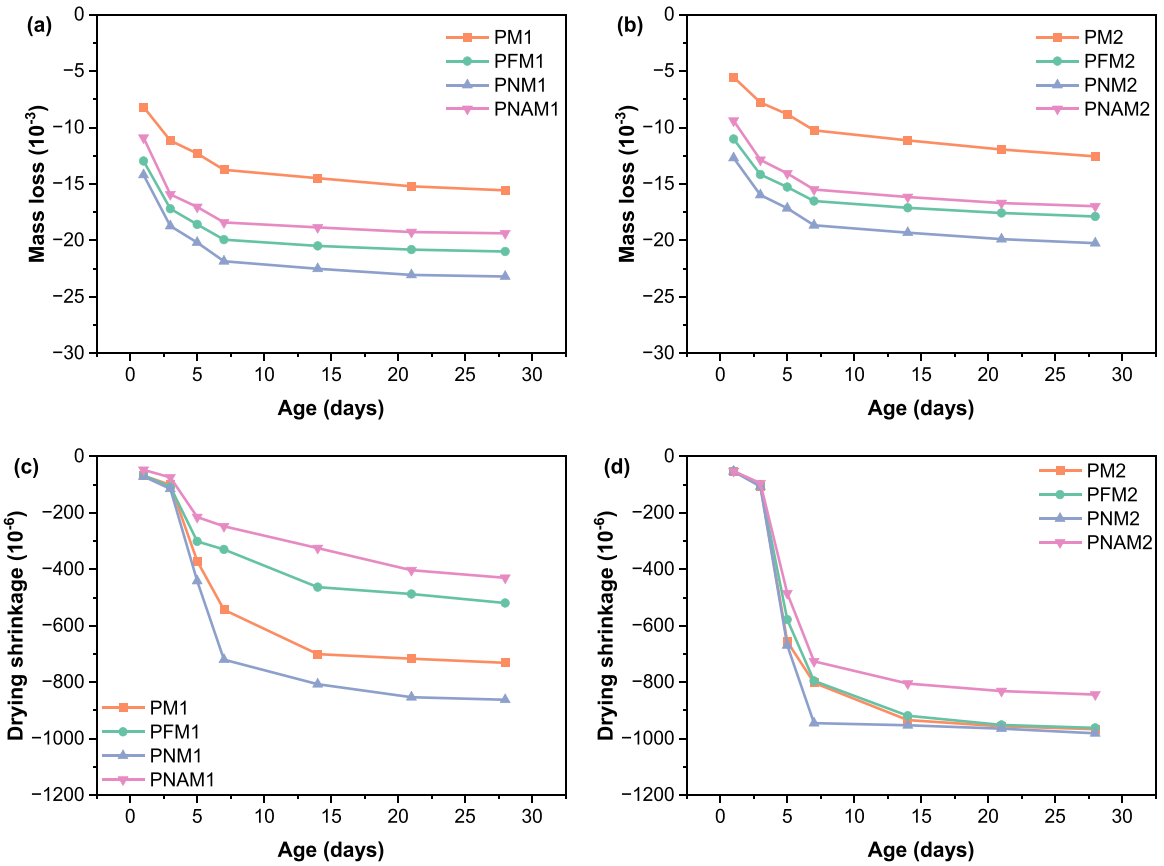

Fig. 8. Mass loss and dry shrinkage of all mortar mixes.

3.3. Compressive and flexural strength

Fig. 9 illustrates the compressive and flexural strength of various mortar mixes at 3 and 28 days. It is evident from Fig. 9 that, within the mortar mixes with the same W/B ratio, the PM group exhibits the highest compressive and flexural strength at 3 days, followed by the PHVNAM, PHVFM, and PHVNM groups. However, at 28 days, the PHVNAM group demonstrates the highest compressive and flexural strength, followed by the PM, PHVFM, and PHVNM groups. This suggests that the inclusion of high-volume FA and NP has a detrimental impact on the mechanical performance of OPC-based mixes. This observation may be attributed to the relatively low content of OPC, which is the primary raw material involved in the hydration reaction. Furthermore, in comparison to the spherical FA particles, which have a water-reducing effect and a positive influence on the hydration reaction [40], that has a good impact on the hydration reaction, the irregular shape of NP particles can absorb the free water that might decrease the relative content of water participating in the hydration reaction [18], leading a lower mechanical strength in the PHVNM group than that the PHVFM group.

With the increasing curing age, the highly active amorphous silica and alumina content in FA or NP may react with hydrated products, improving the mechanical strength of OPC-based mortar mixes. However, compared to FA, the activity of NP participating in the hydration reaction is relatively lower, which further results in the PHVNM group having lower mechanical strength than the PHVFM group, which is even lower than the PM group. Additionally, the mechanical strength of the PHVNM group is enhanced at both 3 and 28 days due to the inclusion of DCA. High-activity silica oxide in DCA, particularly silica fume, contributes to increased hydration reactions [41]. DCA also contains water-retaining composites, which optimize the microstructure of the PHVNM group. This ultimately results in the PHVNAM group with any W/B ratio exhibiting the highest mechanical strength at 28 days.

3.4. Microstructural characterization

3.4.1. Resistivity analysis

It has been reported that the resistivity of cementitious composites undergoes changes as cement hydration progresses, providing a means to describe the hydration process of cementitious composites and assess the influence of mineral additives and chemical additives on cement hydration reactions [42,43]. Fig. 10 presents the electrical resistivity of various cementitious composite pastes over a period of up to 24 h. It is evident from Fig. 10, based on the resistivity development curve of the PP group, that the early-age hydration reaction can be divided into three periods: dissolution and precipitation period (I), induction period (II), and acceleration period (III)

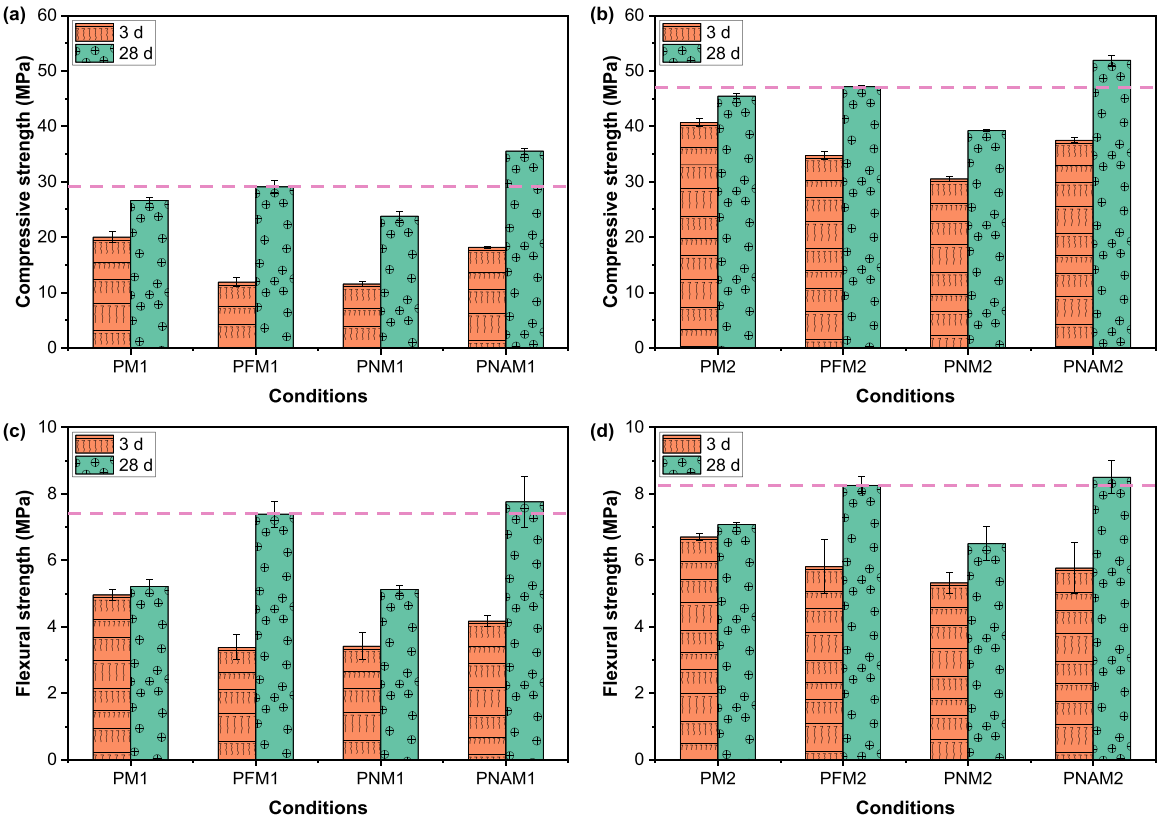

Fig. 9. Compressive strength and flexural strength of different mortars: (a) and (c) concrete with a W/B ratio of 0.49; (b) and (d) concrete with a W/B ratio of 0.38.

[44–46]. The resistivity exhibits a declining trend during the dissolution and precipitation period, primarily influenced by the pore solution containing numerous dissolved ions. Furthermore, there is a gradual increase in resistivity during the induction period, which is mainly due to the continuous dissolution and crystallization of ions in the cementitious materials, with the formation of a protective crystallization layer around the cement particles, preventing further dissolution [47]. Subsequently, as the hydration reaction progresses, more hydration products are generated, leading to a denser porosity, which, in turn, increases the resistivity of the paste matrix [48]. During the acceleration period, a peak is observed, which could be attributed to the intense hydration reactions among various chemical ions, resulting in a reduction in electrical resistivity [49]. After that, as hydration reactions persist, the pores in the cement matrices become filled with hydration products, reducing the porosity of the paste samples and increasing electrical resistivity.

However, it could be clearly noted from Fig. 8 that the time at which the peak occurs in the acceleration period (PIAP) can vary due

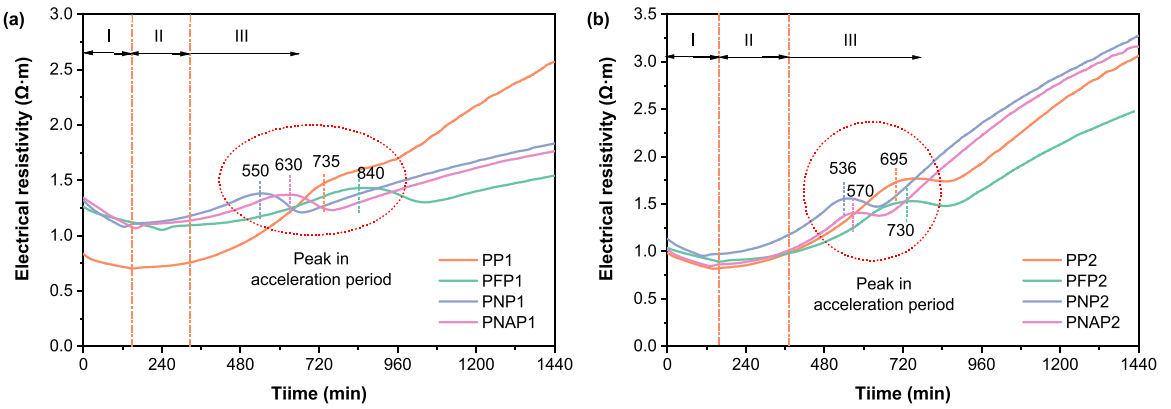

Fig. 10. Electrical resistivity of cementitious composite paste with time up to 24 hrs: (a) different paste with a W/B ratio of 0.49 and (b) different paste with a W/B ratio of 0.35.

to different W/B ratios and FA/NP contents. Referring to Fig. 10, the PIAP appears earlier in the group with a low W/B ratio in comparison to the group with a high W/B ratio. This difference might be attributed to the lower W/B ratio, which results in less water interacting with the hydration reaction and a more stable microstructure, consequently leading to an earlier onset of PIAP. In addition, as shown in Fig. 10, for any group with the same W/B ratio, the onset of the PIAP may occur earlier in the group with NP compared to the group without NP (PP and PHVFP), while the onset of PIAP may be delayed in the group with FA. Simultaneously, incorporating DCA can also delay the onset of PIAP. These observations can be attributed to the following factors: the addition of NP leads to irregularly shaped particles that can absorb free water, reducing the relative water content available for the hydration reaction; spherical FA particles may have a water-reducing effect on the hydration reaction, providing additional water for the hydration process and advancing the onset of PIAP; the inclusion of DCA optimizes the shape of NP particles, reducing their ability to absorb free water, which in turn allows more water to participate in the hydration reaction with cement particles. These observations can be attributed to the following factors [18,40,41]: the addition of NP leads to irregularly shaped particles that can absorb free water, reducing the relative water content available for the hydration reaction; spherical FA particles may have a water-reducing effect on the hydration reaction, providing additional water for the hydration process and advancing the onset of PIAP; the inclusion of DCA optimizes the shape of NP particles, reducing their ability to absorb free water, which in turn allows more water to participate in the hydration reaction with cement particles.

3.4.2. DTA analysis

Fig. 11 presents the DTA curves of all paste mixes at 1 day and 28 days. Based on the DTA curves, it can be observed that there is a thermal effect, with peaks appearing either in an upward (exotherm) or downward (endotherm) direction on the curve [50]. The point where the curve starts to deviate indicates the onset of physical and chemical changes within the sample. The initial peak corresponds to the temperature at which the sample undergoes the most significant changes. The magnitude of the thermal effect is reflected in the height of the peak and the area under the curve [51]. Referring to Fig. 11, the curves for all paste samples indicate the dehydration of various compounds, including C-S-H (at around 100–120 °C), ettringite (AFt, at around 100–120 °C), monosulfate (AFm, at about 160–200 °C), calcium hydroxide (CH, approximately 450–550 °C), and calcite (around 600–800 °C) [52,53]. The addition of FA and NP does not seem to influence the types of hydration products, but it significantly impacts the quantities of generated hydrated products. Notably, the content of CH can be accurately determined through quantitative analysis based on the DTA curves despite the presence of other complex-phase structures.

According to the DTA curves and software analysis, the endothermic peak area (EPA) of CH around 400–500 °C in different paste

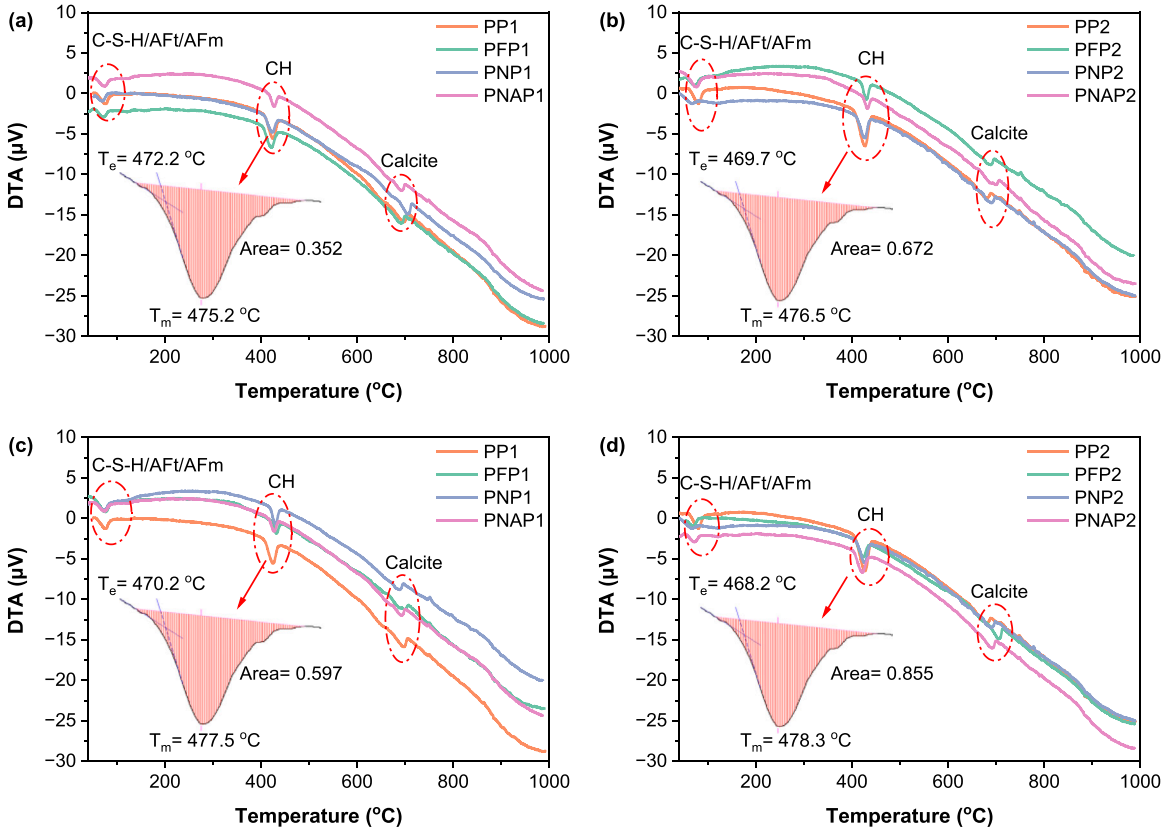

Fig. 11. DTA curve of all paste mixes in different curing ages.

samples was calculated and is presented in Table 5. In this table, we can observe that, within groups sharing the same W/B ratio, the reference groups containing cement have the highest EPA at 1 day. Following them are the groups with NP and DCA, then with FA, and finally NP. In this stage, the generation of CH is mainly generated due to the cement hydration reaction. This might indicate that the addition of DCA can enhance the hydration reaction of the group with NP by optimizing the microstructure. With increasing curing ages, the CH content in all paste samples shows an upward trend. The reference groups have the highest CH content, followed by the group with NP, with FA, and with NP and DCA. The increase in CH content is likely due to the ongoing hydration reactions. However, the varying CH content in the groups with high-volume FA or NP may be attributed to pozzolanic reactions between CH and highly active silica or alumina [54]. The relatively high silica oxide content in FA, as shown in Table 1, leads to more consumption of CH in the group with FA due to pozzolanic reactions. Additionally, the addition of DCA, which also contains highly active silica fume, results in a more significant consumption of CH in the group with NP and DCA compared to the group with FA. Furthermore, the group with a low W/B ratio has a higher cement content, which contributes to a consistently higher CH content than in the group with a high W/B ratio.

3.4.3. SEM analysis

To understand the impact of NP, FA, and DCA on the microstructure of the cement matrices, SEM images of paste samples with a W/B ratio of 0.38 at 1 day and 28 days are presented in Fig. 12 and Fig. 13, respectively. The SEM images in Fig. 12 and Fig. 13 reveal that various hydration products, such as hexagonal-like CH, needle-like AFt, and flocculent C-S-H gels, are present in all samples at 1 day and 28 days. However, in the paste samples with FA, hydrocalumite-like AFm is predominantly detected. This observation may be attributed to the higher content of highly active alumina in FA, as shown in Table 1. The elevated alumina content can trigger the transformation from AFt to AFm, resulting in a more significant generation of AFm [55]. Additionally, due to the high content of FA and NA, the relative content of cement, the primary component for hydration reactions, is decreased. This leads to a narrower range of hydration products and a less dense microstructure in samples with FA or NA.

As shown in Fig. 12 and Fig. 13, compared to the mixes with cement, there are more pores in the group with FA or NA. Moreover, the paste mix with NP exhibits more pores and a relatively looser microstructure than the mixes with FA. However, the addition of DCA optimizes the microstructural properties of the group with NP, resulting in denser and fewer pores detected in the mixes with NP and DCA. These observations provide reasonable explanations for the optimizing effect of DCA on the microstructural properties, which ultimately enhances the shrinkage performance of the group with high-volume NP. Meanwhile, the comparison between Fig. 12 and Fig. 13 reveals that the microstructural properties of the samples at 28 days are denser than those at 1 day. This observation confirms that the mortar mixes experience less change in terms of dry shrinkage and mass loss as the curing age increases, as demonstrated in Fig. 8.

4. Mechanism discussions

The holistic view presented in Fig. 14 provides a comprehensive understanding of the impact of FA, NP, and DCA on the shrinkage performance of concrete with high-volume SCMs. This study shows that the reference group with cement has superior early-age and dry shrinkage performance compared to the groups with FA or NP. This is mainly attributed to the high-volume content of FA and NP, which decreases the relative cement content that primarily participates in the hydration reaction, thereby adversely affecting the shrinkage performance of the concrete. Considering the high value-added aspect of reducing carbon dioxide emissions through the high-volume addition of FA and NP, the effect of FA, NP, and DCA on concrete shrinkage is discussed in this section.

The effect of FA on the early-age shrinkage performance, as depicted in Fig. 14, can be attributed to the spherical nature of FA particles, which resemble a spherical ball. This characteristic has a ball-bearing-like impact, reducing the aggregation of cement particles and facilitating the hydration reaction between cement particles and free water [56]. Although a relatively high content of fly ash decreases the relative cement content, as cement is a primary raw material participating in hydration reactions, the early-age anti-cracking performance of concrete with FA is better than that with NP. As curing ages increase, the ball-bearing effect of FA may optimize microstructural performance and enhance cement hydration reactions, ultimately resulting in the concrete mix with FA exhibiting lower mass loss and drying shrinkage at 28 days compared to that with NP. In addition, in terms of the effect of NP on the early-age shrinkage performance, as shown in Fig. 14, the irregular shape of NP particles is a key factor. These irregular particles might induce water migration among the cement particles and increase the likelihood of aggregation, which can have an adverse effect on hydration reactions [57]. This results in a looser microstructure and the lowest anti-cracking performance among the various concrete mixes. With increasing curing ages, even though NP contains a relatively high content of amorphous silica and alumina, its water-migration effect can still hinder hydration acceleration compared to FA. Consequently, concrete mixes with NP continue to exhibit higher mass loss and drying shrinkage compared to other groups.

As depicted in Fig. 14, regarding the effect of DCA on the early-age shrinkage performance of concrete with high-volume NP, the

Table 5
The Endothermic peak area in the range of 400–500℃.

Mix ID	W/B=0.49				W/B=0.38			
	PP1	PHVFP1	PHVNP1	PHVNAP1	PP2	PHVFP2	PHVNP2	PHVNAP2
1 day	0.353	0.161	0.133	0.185	0.672	0.337	0.276	0.368
28 days	0.597	0.260	0.391	0.229	0.855	0.464	0.608	0.435

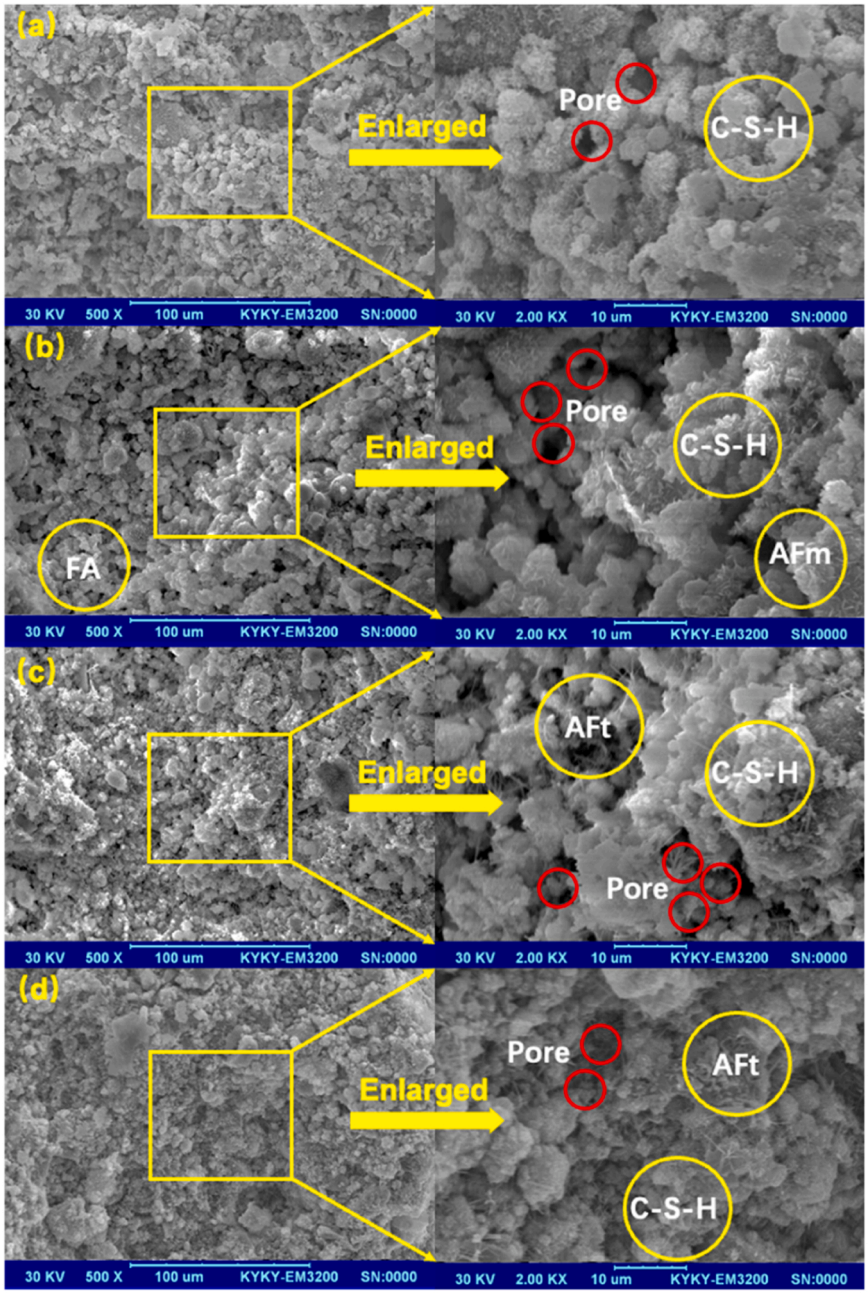

Fig. 12. SEM images of the paste mixes with a W/B of 0.38 in 1 day.

DCA consists of rubber powder, water-retaining agents, and water-reducing agents, such as polyvinyl alcohol and polycarboxylic acid powder. These components can help optimize the irregular surface of NP particles, reducing aggregation among cement particles and enhancing the hydration reaction [24]. This optimization improves the microstructural characteristics of the NP-containing mixes and results in better early-age anti-cracking performance compared to mixes with NP alone and even those with FA. With increasing curing ages, DCA's comprehensive optimisation effects further enhance the NP-containing mixes' microstructural performance. Additionally, the high active content of silica fume in DCA contributes to stronger hydration reactions, leading to lower mass loss and drying shrinkage compared to mixes with NP or FA. In summary, the addition of DCA plays a crucial role in enabling the widespread use of high-volume NP in real-world engineering applications. DCA's optimization effects on the microstructure and hydration reactions of NP-containing concrete enhance the early-age anti-cracking performance and long-term durability of such concrete mixes, making them a feasible and sustainable choice for construction projects.

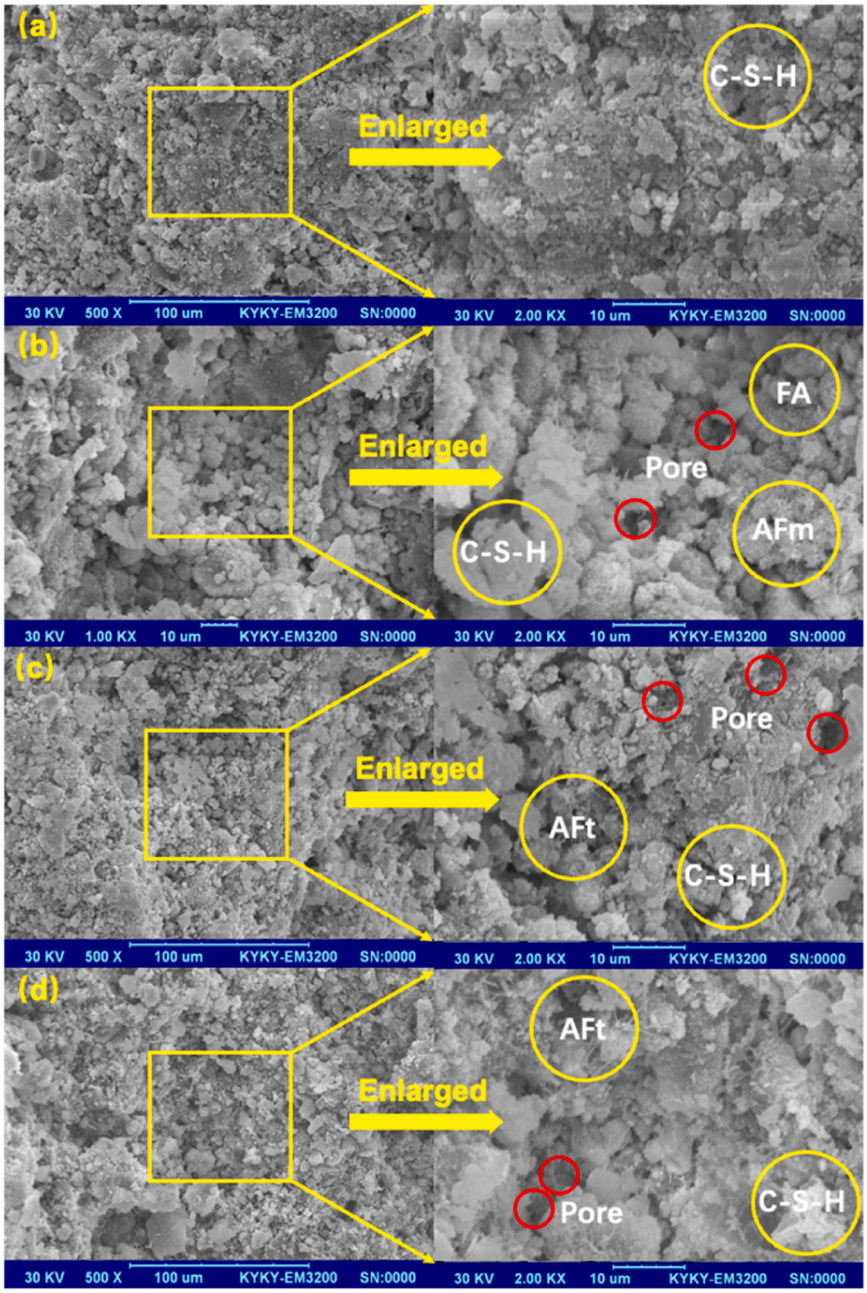

Fig. 13. SEM images of the paste mixes with a W/B of 0.38 in 28 days.

5. Conclusions

Considering the abundance of NP resources in the high-speed railway between Dali and Ruili in Yunnan Province, China, this study used the NP to replace the FA in sustainable concrete production for high-speed railway design. However, due to NP's low pozzolan reactivity index, the NP's large-scale application in sustainable concrete with high-volume NP content is limited. Therefore, a designed composite agent was employed to enhance the shrinkage performance of the concrete with high-volume NP. Based on the early-age shrinkage performance evaluation, drying shrinkage performance evaluation, phase transformations and microstructural performance evaluation, some conclusions were drawn in the following:

1) The addition of DCA can improve the early-age cracking performance of the mixes with high-volume NP content, resulting in a lower crack density found in the mixes with NP and DCA, than in other mixes with SCMs content.

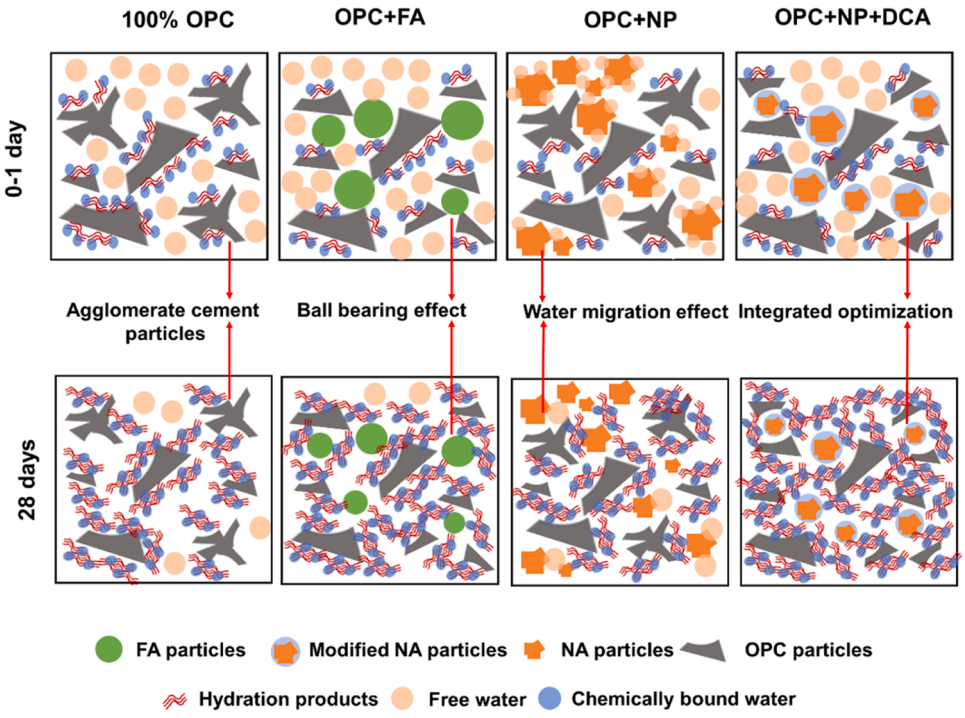

Fig. 14. Schematic diagram of mechanism about the effect of the FA, NP, and DCA on the shrinkage performance.

2) The addition of DCA can also enhance the drying shrinkage performance of the mixes with high-volume NA content, where the mixes with both NP and DCA have a lower dry shrinkage and mass loss than other mixes with NP or FA content.
3) The addition of DCA can also increase the compressive and flexural strength of the mixes with high-volume NP, leading the mixes with both NP and DCA to have the highest 28-day compressive and flexural strength than other mixes with NP or FA, even higher than the reference mixes with OPC.
4) The resistivity analysis results demonstrated that the addition of DCA can optimize the shape of the NP particles and ensure more free water can participate in the hydration reaction, further delaying the onset of the peak in the acceleration period of the mixes with NP.
5) The DTA and SEM analysis also showed that the addition of DCA can also increase the hydration reaction due to the content of silica fume in DCA and generate much more hydration products, optimizing the microstructure performance of the mixes with high-volume NP, further improving the shrinkage and mechanical performance of the sustainable concrete with high-volume NP.

CRediT authorship contribution statement

Fulin Qu: Writing – review & editing, Writing – original draft, Data curation. **Yilin Su:** Writing – review & editing, Writing – original draft, Supervision, Methodology. **Dong Lu:** Writing – review & editing, Methodology. **Ning Li:** Methodology, Writing – review & editing. **Xiaohui Zeng:** Writing – review & editing. **Wengui Li:** Writing – review & editing, Supervision, Methodology.

Declaration of Competing Interest

The authors declare that they have no known competing financial interests or personal relationships that could have appeared to influence the work reported in this paper.

Data availability

Data will be made available on request.

Acknowledgments

The authors appreciate the support from the Australian Research Council (ARC), Australia (FT220100177; LP230100288; DP220101051; IH180100010; DP220100036).

References

[1] A. Mohammadi, A.M. Ramezanianpour, Investigating the environmental and economic impacts of using supplementary cementitious materials (SCMs) using the life cycle approach, J. Build. Eng. (2023) 107934.
[2] Z. Wan, T. He, S. Wan, N. Chang, X. Ma, H. Qiu, Study on the effect of supplementary cementitious materials on the volume stability of mortar mixed with laboratory-made high-content fluorine-type accelerator, J. Build. Eng. 69 (2023) 106166.
[3] Y. Liu, Y. Zhuge, X. Chen, W. Duan, R. Fan, L. Outhred, L. Wang, Micro-chemomechanical properties of red mud binder and its effect on concrete, Compos. Part B: Eng. 258 (2023) 110688.
[4] H. Zong, Y. Wang, G. Wang, Q. Li, F. Li, Q. Li, P. Hou, The role of ultra-fine supplementary cementitious materials in the durability and microstructure of airport pavement concrete, Constr. Build. Mater. 392 (2023) 131954.
[5] R. Snellings, P. Suraneni, J. Skibsted, Future and emerging supplementary cementitious materials, Cem. Concr. Res. 171 (2023) 107199.
[6] F. Qu, W. Li, X. Zeng, Z. Luo, K. Wang, D. Sheng, Effect of microlimestone on properties of self-consolidating concrete with manufactured sand and mineral admixture, Front. Struct. Civ. Eng. 14 (2020) 1545–1560.
[7] V. Shobeiri, B. Bennett, T. Xie, P. Visintin, Mix design optimization of concrete containing fly ash and slag for global warming potential and cost reduction, Case Stud. Constr. Mater. 18 (2023) e01832.
[8] F. Qu, W. Li, Y. Guo, S. Zhang, J.L. Zhou, K. Wang, Chloride-binding capacity of cement-GGBFS-nanosilica composites under seawater chloride-rich environment, Constr. Build. Mater. 342 (2022) 127890.
[9] J. Ding, S. Ma, S. Shen, Z. Xie, S. Zheng, Y. Zhang, Research and industrialization progress of recovering alumina from fly ash: a concise review, Waste Manag. 60 (2017) 375–387.
[10] I. Diaz Loya, M. Juenger, S. Seraj, R. Minkara, Extending supplementary cementitious material resources: reclaimed and remediated fly ash and natural pozzolans, Cem. Concr. Compos. 101 (2019) 44–51.
[11] S. Dai, D. Ren, Y. Zhou, C.L. Chou, X. Wang, L. Zhao, X. Zhu, Mineralogy and geochemistry of a superhigh-organic-sulfur coal, Yanshan Coalfield, Yunnan, China: evidence for a volcanic ash component and influence by submarine exhalation, Chem. Geol. 255 (1-2) (2008) 182–194.
[12] L. Yu, S. Zhou, J. Dong, Investigation into pozzolanic activity component of basalt and pumice, J. Mater. Civ. Eng. 32 (6) (2020) 04020135.
[13] L. Wang, F. Guo, Y. Lin, H. Yang, S. Tang, Comparison between the effects of phosphorous slag and fly ash on the CSH structure, long-term hydration heat and volume deformation of cement-based materials, Constr. Build. Mater. 250 (2020) 118807.
[14] H. Wang, C. Ju, M. Zhou, Y. Dong, H. Hou, S. Liu, Grinding kinetics of lead–zinc tailing powders and its optimal particle size as a pozzolanic admixture in cement mortar, Adv. Powder Technol. 33 (9) (2022) 103730.
[15] C. Wu, Investigation of foundation theory of safety & security complexity, J. Saf. Sustain. (2023).
[16] M. Zhang, X. Zhu, S. Pyo, Y. Yang, B. Liu, J. Shi, Feasibility of using high-volume pozzolanic fillers to develop sustainable engineered cementitious composites (ECC), Powder Technol. 428 (2023) 118853.
[17] M.U. Hossain, R. Cai, S.T. Ng, D. Xuan, H. Ye, Sustainable natural pozzolana concrete–a comparative study on its environmental performance against concretes with other industrial by-products, Constr. Build. Mater. 270 (2021) 121429.
[18] J.C. Liu, M.U. Hossain, S.T. Ng, H. Ye, High-performance green concrete with high-volume natural pozzolan: mechanical, carbon emission and cost analysis, J. Build. Eng. 68 (2023) 106087.
[19] W. Wilson, J. Rivera-Torres, L. Sorelli, A. Durán-Herrera, A. Tagnit-Hamou, The micromechanical signature of high-volume natural pozzolan concrete by combined statistical nanoindentation and SEM-EDS analyses, Cem. Concr. Res. 91 (2017) 1–12.
[20] F. Liu, S.L. Shen, D.W. Hou, A. Arulrajah, S. Horpibulsuk, Enhancing behavior of large volume underground concrete structure using expansive agents, Constr. Build. Mater. 114 (2016) 49–55.
[21] K. Celik, M.D. Jackson, M. Mancio, C. Meral, A.H. Emwas, P.K. Mehta, P.J.M. Monteiro, High-volume natural volcanic pozzolan and limestone powder as partial replacements for portland cement in self-compacting and sustainable concrete, Cem. Concr. Compos. 45 (2014) 136–147.
[22] K. Celik, C. Meral, M. Mancio, P.K. Mehta, P.J.M. Monteiro, A comparative study of self-consolidating concretes incorporating high-volume natural pozzolan or high-volume fly ash, Constr. Build. Mater. 67 (2014) 14–19.
[23] M. Sharbaf, M. Najimi, N. Ghafoori, A comparative study of natural pozzolan and fly ash: investigation on abrasion resistance and transport properties of self-consolidating concrete, Constr. Build. Mater. 346 (2022).
[24] S. Ahmad, K.O. Mohaisen, S.K. Adekunle, S.U. Al-Dulaijan, M. Maslehuddin, Influence of admixing natural pozzolan as partial replacement of cement and microsilica in UHPC mixtures, Constr. Build. Mater. 198 (2019) 437–444.
[25] G. Long, Y. Chen, Z. Tang, M. Shangguan, C. Gao, S. Xu, Drying shrinkage behavior of cement mortar under low vacuum conditions, Constr. Build. Mater. 374 (2023) 130933.
[26] N.P. Tran, C. Gunasekara, D.W. Law, S. Houshyar, S. Setunge, A. Cwirzen, A critical review on drying shrinkage mitigation strategies in cement-based materials, J. Build. Eng. 38 (2021) 102210.
[27] L. Ma, Y. Zhao, J. Gong, Restrained early-age shrinkage cracking properties of high-performance concrete containing fly ash and ground granulated blast-furnace slag, Constr. Build. Mater. 191 (2018) 1–12.
[28] J. Kheir, A. Klausen, T.A. Hammer, L. De Meyst, B. Hilloulin, K. Van Tittelboom, A. Loukili, N. De Belie, Early age autogenous shrinkage cracking risk of an ultra-high performance concrete (UHPC) wall: modelling and experimental results, Eng. Fract. Mech. 257 (2021) 108024.
[29] F. Qu, H. Zhao, K. Wu, Y. Liu, X. Zhao, W. Li, Phase transformation and microstructure of in-situ concrete after 20-year exposure to harsh mining environment: a case study, Case Stud. Constr. Mater. 19 (2023) e02287.
[30] T. Du, C. Li, X. Wang, L. Ma, F. Qu, B. Wang, J. Peng, W. Li, Effects of pipe diameter, curing age and exposure temperature on chloride diffusion of concrete with embedded PVC pipe, J. Build. Eng. 57 (2022) 104957.
[31] T. Tioua, A. Kriker, G. Barluenga, I. Palomar, Influence of date palm fiber and shrinkage reducing admixture on self-compacting concrete performance at early age in hot-dry environment, Constr. Build. Mater. 154 (2017) 721–733.
[32] N.F. Medina, G. Barluenga, F. Hernández-Olivares, Enhancement of durability of concrete composites containing natural pozzolans blended cement through the use of Polypropylene fibers, Compos. Part B: Eng. 61 (2014) 214–221.
[33] J. Zhang, Y. Yan, Z. Hu, X. Xie, L. Yang, Properties and hydration behavior of Ti-extracted residues-red gypsum based cementitious materials, Constr. Build. Mater. 218 (2019) 610–617.
[34] Y. Su, L. Wu, X. He, Z. Zheng, H. Tan, J. Yang, Q. Ma, J. Ding, M. Bao, A novel early strength agent prepared by wet-grinding concrete waste slurry and its effect on early hydration and mechanical properties of cement based materials, Constr. Build. Mater. 362 (2023) 129673.
[35] Q. Xiao, Y. Cai, G. Long, K. Ma, X. Zeng, Z. Tang, W. Li, H. Wang, J. Peng, Effect of alternating current curing on properties of carbon black-cement conductive composite: Setting, hydration and microstructure, J. Build. Eng. 72 (2023) 106603.
[36] S. Patel, A. Orlov, E. Ariyachandra, S. Peethamparan, Effect of flue gas temperature on NO2 adsorption by aged recycled concrete waste: DRIFTS, TGA and BET study, Chem. Eng. J. 420 (2021) 130413.
[37] T. Yang, Z. Zhang, H. Zhu, W. Zhang, Y. Gao, X. Zhang, Q. Wu, Effects of calcined dolomite addition on reaction kinetics of one-part sodium carbonate-activated slag cements, Constr. Build. Mater. 211 (2019) 329–336.
[38] Y. Guo, W. Li, W. Dong, Z. Luo, F. Qu, F. Yang, K. Wang, Self-sensing performance of cement-based sensor with carbon black and polypropylene fibre subjected to different loading conditions, J. Build. Eng. 59 (2022) 105003.
[39] W. Dong, W. Li, Y. Guo, Z. Sun, F. Qu, R. Liang, S.P. Shah, Application of intrinsic cement-based sensor for traffic detections of human motion and vehicle speed, Constr. Build. Mater. 355 (2022) 129130.
[40] I. Cavusoglu, E. Yilmaz, A.O. Yilmaz, Additivity effect on properties of cemented coal fly ash backfill containing water-reducing admixtures, Constr. Build. Mater. 267 (2021) 121021.

[41] Y. Lou, K. Khan, M.N. Amin, W. Ahmad, A.F. Deifalla, A. Ahmad, Performance characteristics of cementitious composites modified with silica fume: a systematic review, Case Stud. Constr. Mater. (2022) e01753.
[42] J. Deng, X. Zhu, D. Xiong, Q. Li, C. Yang, K. Yang, M. Basheer, Mitigation of autogenous shrinkage of alkali-activated slag mortar by stearate salts, Constr. Build. Mater. 384 (2023) 131383.
[43] Y. Zhang, H. Li, A. Abdelhady, J. Yang, Comparative laboratory measurement of pervious concrete permeability using constant-head and falling-head permeameter methods, Constr. Build. Mater. 263 (2020) 120614.
[44] L. Huang, L. Tang, H. Gu, Z. Li, Z. Yang, New insights into the reaction of tricalcium silicate (C3S) with solutions to the end of the induction period, Cem. Concr. Res. 152 (2022) 106688.
[45] X. Zeng, H. Liu, H. Zhu, C. Ling, K. Liang, H. Umar, Y. Xie, G. Long, C. Ma, Study on damage of concrete under uniaxial compression based on electrical resistivity method, Constr. Build. Mater. 254 (2020) 119270.
[46] K. Liang, X. Zeng, X. Zhou, C. Ling, P. Wang, K. Li, S. Ya, Investigation of the capillary rise in cement-based materials by using electrical resistivity measurement, Constr. Build. Mater. 173 (2018) 811–819.
[47] K. Liang, X. Zeng, X. Zhou, F. Qu, P. Wang, A new model for the electrical conductivity of cement-based material by considering pore size distribution, Mag. Concr. Res. 69 (20) (2017) 1067–1078.
[48] J. Chen, Z. Li, X. Jin, Critical features of microstructure development of early-age cement paste revealed by non-contact electrical resistivity measurement, Constr. Build. Mater. 154 (2017) 1121–1129.
[49] Y. Lu, J. Zhang, Z. Li, Study on hydration process of early-age concrete using embedded active acoustic and non-contact complex resistivity methods, Constr. Build. Mater. 46 (2013) 183–192.
[50] V. Lilkov, O. Petrov, Y. Tzvetanova, P. Savov, Mössbauer, DTA and XRD study of Portland cement blended with fly ash and silica fume, Constr. Build. Mater. 29 (2012) 33–41.
[51] M.S. Kim, Y. Jun, C. Lee, J.E. Oh, Use of CaO as an activator for producing a price-competitive non-cement structural binder using ground granulated blast furnace slag, Cem. Concr. Res. 54 (2013) 208–214.
[52] D.C. Chu, J. Kleib, M. Amar, M. Benzerzour, N.-E. Abriak, Determination of the degree of hydration of Portland cement using three different approaches: scanning electron microscopy (SEM-BSE) and Thermogravimetric analysis (TGA), Case Stud. Constr. Mater. 15 (2021) e00754.
[53] W. Deboucha, N. Leklou, A. Khelidj, M.N. Oudjit, Hydration development of mineral additives blended cement using thermogravimetric analysis (TGA): methodology of calculating the degree of hydration, Constr. Build. Mater. 146 (2017) 687–701.
[54] D.O. Koteng, C.T. Chen, Strength development of lime–pozzolana pastes with silica fume and fly ash, Constr. Build. Mater. 84 (2015) 294–300.
[55] R. Mistry, T.K. Roy, Performance evaluation of bituminous mix and mastic containing rice husk ash and fly ash as filler, Constr. Build. Mater. 268 (2021) 121187.
[56] E. Khankhaje, T. Kim, H. Jang, C. Kim, J. Kim, Properties of pervious concrete incorporating fly ash as partial replacement of cement: a review, Dev. Built Environ. (2023) 100130.
[57] S. Ahmad, O.S.B. Al-Amoudi, S.M. Khan, M. Maslehuddin, Effect of silica fume inclusion on the strength, shrinkage and durability characteristics of natural pozzolan-based cement concrete, Case Stud. Constr. Mater. 17 (2022) e01255.